scientific reports

Check for updates

OPEN

Study on pore structure and adsorption properties of coal and microscopic action mechanism of outburst

Peng Zou[1], Anying Yuan[1]✉, Bing Zhang[2], Huaqiang Liu[1], Kang Jin[1] & Hao Zhong[1]

Coal and gas outburst is a complex dynamic phenomenon happened in the underground of coal mines, and it has been a serious threat to the safe and efficient production of mines. To investigate the intricate mechanisms at play, a large-scale coal and gas outburst test was conducted based on the prototype of outbursts induced by coal uncovering. Coal samples were obtained through isometric excavation, grinding, and sieving, followed by an analysis of their pore structure and gas adsorption properties. Furthermore, the microscopic mechanisms underlying the disaster caused by the deterioration of coal due to the combined effects of in-situ stress and gas pressure were examined using fracture mechanics theory. The research findings aim to enhance the foundational theory of coal and gas outbursts and provide technical references for prevention efforts.

Keywords Coal and gas outburst, Physical simulation, Pore structure, Gas absorption property, Outburst mechanism

As shallow resources become increasingly depleted, the demand for deeper resources has become an inevitable trend. However, the challenging con-ditions of deep coal resources, complex geological mining conditions, rising in-situ stress, and significantly increased gas content in coal seams have led to greater intensity and frequency of dynamic disasters. This situation poses a major threat to the safe and efficient mining operations in mines[1–3]. Coal and gas outburst is a type of dynamic disaster that occurs in underground coal mines, characterized by complex instability phenomena. Once initiated, it can suddenly eject fragmented coal bodies and release a large volume of gas into the mining space, leading to sig-nificant damage to facilities, mine shutdowns, and other serious consequences[4–6]. Therefore, studying the development process of coal and gas outbursts and exploring the interaction mechanisms of their internal factors is essential.

In view of the fact that coal and gas outburst is a complex dynamic disaster that occurs underground in coal mines, coupled with the fact that the outburst has space limitation and time instantaneity, it leads to field research becoming difficult and it is hard to accurately characterize the mechanism of its occurrence, so physical simulation experiment is carried out to become an important way and a scientific mean to study coal and gas outburst[7–9]. Many scholars have used different scales of coal and gas outburst equipment to study the conventional physical parameters in the process of outburst, such as gas pressure and its permeability[10–12], in-situ stress[13], spalling[14], and the distribution of the outbursting coal dust[15], and the unconventional physical parameters, such as the energy evolution[16], the information of outburst precursors[17], the adsorption and desorption properties of gas in coal[18], and the effective stress[19], etc. have been studied, in addition, the theoretical model of outburst disaster or the mechanism of action of outburst catastrophe has been established by some of these scholars from the change rule of physical parameters.It can be seen that it is feasible and effective to use physical simulation devices to study the in-situ stress, gas pressure, and physical properties of the coal during coal and gas outburst, and then explore the complex action mechanism of the process, but at present the relevant internal mechanism and theoretical model have not been accurately finalized, and there are still many valuable contents that need to be further explored.

Given that coal and gas outburst is a complex dynamic disaster that occurs underground in coal mines, and considering its spatial limitations and instantaneous nature, field research becomes challenging, making it difficult to accurately characterize the mechanism of its occurrence. Therefore, conducting physical simulation

[1]State Key Laboratory Mine Response and Disaster Prevention and Control in Deep Coal Mine, Anhui University of Science and Technology, Huainan 232001, China. [2]Geotechnical and Structural Engineering Research Centre, Shandong University, Jinan 250061, China. ✉email: ayyuan@aust.edu.cn

experiments has become an important and scientific method for studying coal and gas outburst[7–9]. Many scholars have employed various scales of coal and gas outburst equipment to study conventional physical parameters during the outburst process, such as gas pressure and permeability[10–12], in-situ stress[13], spalling[14], and the distribution of outbursting coal dust[15]. They have also investigated unconventional physical parameters, including energy evolution[16], information about outburst precursors[17], the adsorption and desorption properties of gas in coal[18], and effective stress[19]. It is evident that studying in-situ stress, gas pressure, and the physical properties of coal during coal and gas outbursts using physical simulation devices is both feasible and effective. Additionally, some scholars have established theoretical models of outburst disasters or explored the mechanisms behind these phenomena based on the changing patterns of individual physical parameters, yielding many valuable experimental results. However, the complex interplay of various physical factors affecting coal and gas outbursts has led to a lack of uniformity in the established theoretical models, indicating that further exploration is still needed.

In addition, due to the sudden, dangerous, and concealed nature of coal and gas outbursts, only limited information related to the process can be obtained in the field[20–23], but this information is the key factor to study the mechanism of the outburst. While the mechanism of the outburst has been studied from the macroscopic phenomenon by establishing physical or mathematical models to describe and quantify its unique physical structure, the coal at the microscopic scale also has unique physical characteristics and the outburst process is closely related to it[24–26]. Changes in physical states such as the in-situ stress conditions at the location of the coal seam, the adsorption and desorption properties of the gas, and the failure characteristics of the coal will inevitably cause the internal pores and cracks of the coal to change[27,28]. The study of the structure of microscopic pores and cracks in coal and the state of internal gas concentration is essential to grasp and understand the whole process of outburst from initiation to termination.The pore structure of coal with different degrees of metamorphism or types of coal is often studied by low-temperature liquid nitrogen adsorption method[29–31], while the adsorption and desorption properties of coal are obtained by gas adsorption method[32,33], and it can be seen from the results of the existing research, the pore structure and adsorption properties of coal samples after the action of different conditions are changed to a different extent[34–37].This suggests that the pore structure of coal, as well as the storage state and migration mode of the gas within it, have an impact on the properties of coal, especially the potential effect on the outburst process, which cannot be ignored. Therefore, it is an essential research path to understand and explore the mechanism of coal and gas outbursts by studying the microscopic pore structure of the outburst coal and the characteristics of the existence and flow characteristics of the gas therein.

In addition, due to the sudden, hazardous, and concealed nature of coal and gas outbursts, only limited information related to the process can be obtained in the field[20–23]. However, this infor-mation is crucial for understanding the mechanism of outbursts. While the outburst mechanism has been studied from a macroscopic perspective by estab-lishing physical or mathematical models to describe and quantify its distinctive physical structure, coal at the microscopic scale also exhibits unique physical characteristics, and the outburst process is closely linked to these properties[24–26]. Changes in phys-ical states, such as in-situ stress conditions at the coal seam, the adsorption and desorption properties of gas, and the failure characteristics of coal, inevitably alter the internal pores and cracks within the coal[27,28]. Studying the structure of microscopic pores and cracks in coal and the state of internal gas concen-tration is essential to comprehensively understand the entire outburst process from initiation to termination. The pore structure of coal with varying degrees of metamorphism or different coal types is often studied using the low-temperature liquid nitrogen adsorption method[29–31], while the adsorption and desorption properties of coal are determined through gas ad-sorption methods[32,33]. Existing research shows that the pore structure and adsorption properties of coal samples change to varying degrees under dif-ferent conditions[34–37]. This indicates that the pore structure of coal, as well as the storage state and migration mode of the gas within it, significantly impact the coal's properties, particularly its potential effect on the outburst process, which should not be overlooked. However, there are few studies examining the interaction between coal and gas from a microscopic perspective. Therefore, the mechanism of coal and gas outbursts can be better understood by investigating the microscopic pore structure of outburst coal, along with the existing forms and flow characteristics of gas.

In this paper, a large-scale physical similarity simulation test system for coal and gas outbursts is utilized, in conjunction with a specific surface area analyzer and a high-pressure gas adsorption instrument. By collecting outburst coal samples during the test, the internal pore structure and the gas adsorption and desorption characteristics are analyzed. Additionally, the mechanisms underlying the outburst phenomenon are investigated at the microscopic level based on fracture mechanics theory. The research findings aim to enhance the foundational theory of coal and gas outbursts and provide technical references for prevention efforts.

Experimental methods

This study comprises four main tests: (1) a true three-dimensional large-scale coal and gas outburst test; (2) a sampling and crushing test; (3) a low-temperature liquid nitrogen adsorption test; and (4) a high-pressure gas adsorption and desorption test. The test process is illustrated in Fig. 1. The primary purpose of Test (1) is to replicate the occurrence of coal and gas outbursts in areas with abnormal coal thickness. Outburst coal samples were collected and crushed after the completion of Test (2). Subsequently, the pore structure (Test 3) and adsorption–desorption characteristics (Test 4) were analyzed using the processed coal samples, focusing on the characteristics of pore structure and gas adsorption and desorption at varying distances from the outburst outlet.

Real three-dimensional large-scale coal and gas outburst test

A mine in Guizhou utilized an inclined shaft to access the No. 9 coal seam, where the average coal thickness observed from drilling at the wellhead of the extension roadway was 10.3 m. Following a blasting operation, a

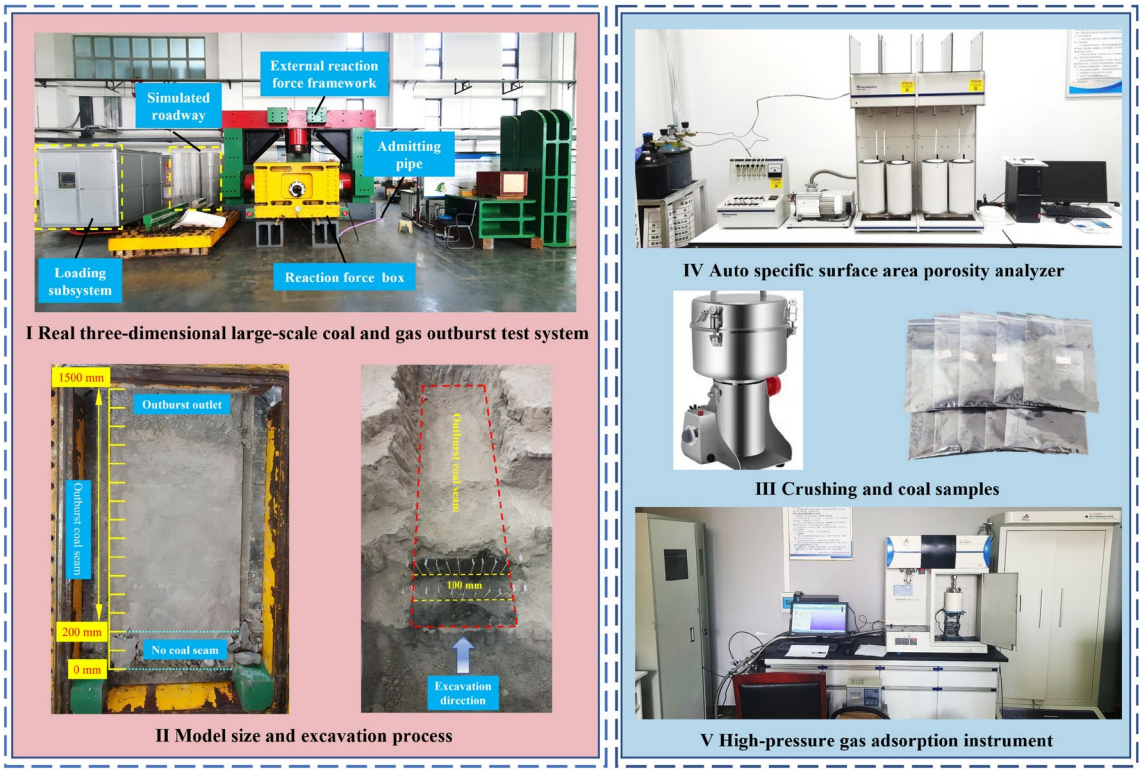

Fig. 1. Determination of pore structure and desorption characteristics of coal and gas outburst coal samples.

coal and gas outburst accident occurred. This incident served as a prototype for further investigation; the coal was processed into briquette coal through field sampling, and a coal and gas outburst test was conducted using a self-developed true three-dimensional large-scale physical simulation test system (Fig. 1). The system primarily consists of a power loading subsystem, an external against-force frame, an against-force box (dimensions: 1500 mm × 800 mm × 800 mm), a gas-filling subsystem, and an information collection subsystem, as illustrated in Fig. 1 (I).

By combining the case prototype with the dimensions of the against-force box and applying similarity theory, the geometric similarity ratio $C_L = 12.5$, bulk density scale $C_\gamma = 1$, and in-situ stress scale $C_\sigma = 12.5$ were determined. The depth of the coal seam is approximately 1100 m, with an average bulk density of 2.5 g/cm^3 and a maximum gas pressure of 1.13 MPa. Using the formula for vertical stress $\sigma_v = \gamma H = 27.5$ MPa, and taking the stress concentration factor as 0.6, the horizontal stress is calculated as $\sigma_2 = \sigma_3 = 0.6\gamma H = 16.5$ MPa. These stresses are then applied in all directions to the against-force box. The model setup, in-situ stress application, and software and hardware debugging steps are completed. After evacuating the against-force box, the outburst gas is injected in stages until reaching the set critical pressure value (According to the field data, the critical pressure for the design test is 1 MPa), at which point the outburst is initiated.

Coal samples crushing and acquisition test

After the outburst test, manual excavation was employed to minimize secondary damage to the outburst coal sample and to maintain its original state as much as possible. Excavation commenced from the back of the against-force box toward the outburst direction. First, the reaction box was opened to reveal the top rock formation, exposing the coal seam. Next, the top and middle rock formations within a distance of 0 mm to 200 mm from the outburst outlet were excavated. Finally, the coal and rock formations were excavated in fixed increments of 100 mm, during which outburst coal samples were collected. Because the coal within the range of 200 mm to 400 mm was unbroken, samples from the range of 300 mm to 400 mm were used to represent this interval. The internal shape of the against-force box and the excavation process are illustrated in Fig. 1 (II).

It is worth noting that the coal samples were collected uniformly and distributed according to the principle of multi-point sampling within the unit advancement distance to ensure that the collected samples were representative of their positions. Upon completion of the coal seam excavation, coal samples (60–80 mesh) suitable for pore size analysis and adsorption–desorption tests were obtained through grinding and sieving, as shown in Fig. 1 (III).

Pore structure characterization test

The low-temperature liquid nitrogen adsorption test was conducted on the coal samples using an ASAP 2460 surface area and pore size analyzer, as shown in Fig. 1 (IV). Prior to the test, the samples were degassed under vacuum at 130 °C for more than 8 h to remove volatiles. Following this, the samples were placed into the analyzer,

and the parameters were adjusted to initiate the test. The pore structure characteristics of the samples, including specific surface area and pore volume, were determined using the Barrett-Joyner-Halenda (BJH) model, Density Functional Theory (DFT) model, Brunauer–Emmett–Teller (BET) model, and other models[38–41].

High-pressure gas adsorption test

The adsorption and desorption test was conducted using a 3H-2000PH high-pressure gas adsorption instrument, as shown in Fig. 1 (V). First, the coal samples were weighed and placed into the sample tank for vacuum treatment. Next, the heating furnace was activated to perform the adsorption test. Then, the water levels in the free, desorption, and exhaust water pipes were adjusted sequentially, and the height of the internal liquid level was recorded. Finally, the data were imported into the software to generate a report marking the end of the test.

Experiment results and analysis

Analysis of the hole shape and spallation characteristics of the outburst coal seam

At the conclusion of the coal and gas outburst test, the shape of the coal seam post-outburst was determined by uncovering the top rock formation and completing the excavation process, as shown in Fig. 2.

The shape of the exposed coal seam appears relatively intact, without significant failure. Additionally, the outburst holes along the centerline of the outburst outlet exhibit a "V" morphology, transitioning from a "small mouth with a large cavity" to a "large cavity with a small mouth" as one moves from the outlet into the interior of the box. The front section (Area A) and the rear section (Area B) exhibit outburst and similar extrusion dynamic phenomena, respectively. This behavior can be attributed to the rapid depressurization at the outburst outlet, causing cracks within the initially exposed coal to expand under the influence of in-situ stress and gas pressure. Consequently, the coal in the middle of the exposed surface begins to fracture and destabilize, progressively displacing the surrounding coal. This action creates conditions for the coal at the back, leading to the formation of the outburst hole in Area A during the early stages of the outburst, which gradually enlarges. As the outburst phenomenon continues, a significant amount of coal is ejected from Area A, resulting in gas leakage and the gradual release of energy stored within the coal. This process causes the outburst hole in Area B to gradually diminish until it eventually stops, leading to the formation of a gradually shrinking hole in the late stages. This observation aligns with the phenomena described in reference[42].

After the initiation of the coal and gas outburst, the coal was rapidly fractured, stripped, and ejected due to in-situ stress and gas pressure. Following the outburst, a distinct outburst hole remained in the against-force box, while spalling features were exhibited by the layer lobes that had been peeled off but not expelled, still present within the hole (Fig. 3).

The evolution characteristics of the spalling structure of the coal in the outburst hole are shown in Fig. 3. It can be seen that the coal in the rear section of the outburst hole is destroyed, and an obvious spalling phenomenon occurs, at this time, the direction of spalling is mostly perpendicular to the direction of the outburst, which shows typical tensile failure characteristics. With the increase of advancing distance, the direction of spalling began to shift after entering the front section of the outburst hole, this phenomenon was especially obvious near the outburst outlet, and the direction of spalling gradually made an acute angle with the direction of the outburst outlet, which showed a hemispherical distribution morphology. The principle of the "spherical shell instability" hypothesis can be explained: when the outburst outlet is quickly opened, under the action of in-situ stress, the principal stress in the coal seam nearby is distributed in a hemispherical shape, and at the same time, type I cracks of the same morphology are generated; under the action of gas pressure, the cracks' tip gradually expands and eventually forms the shape of a spherical crown, and the coal in the near area of outburst outlet is peeled off and thrown out along the spherical crown cracks after the initiation of the outburst. After the initiation of the outburst, the coal is peeled off and thrown out along the bulbous crown cracks. During the continuous occurrence and attenuation of outburst, the energy to maintain the outburst is gradually released, which will weaken the phenomenon of outburst, and at the same time, a large number of broken coal fragments left in

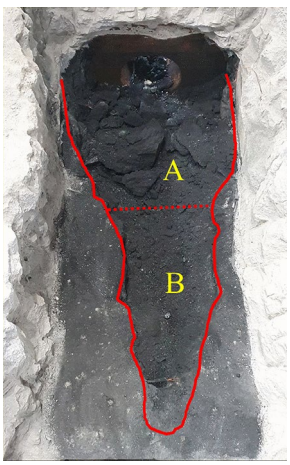

Fig. 2. Coal and gas outburst hole shape.

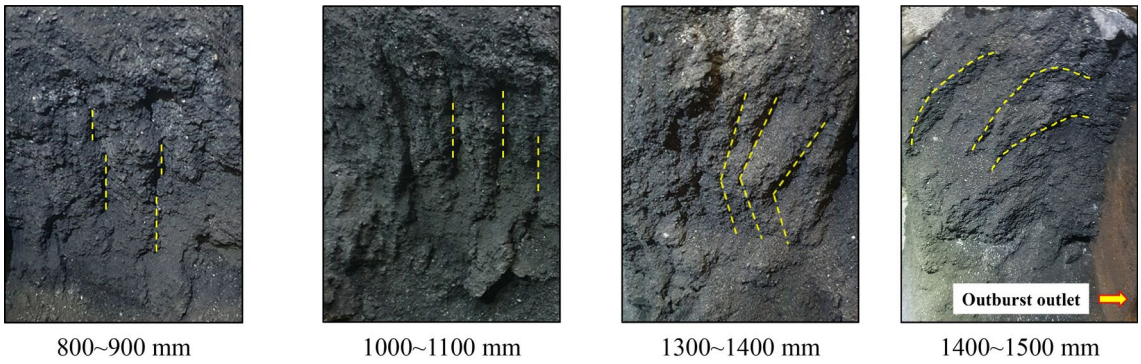

Fig. 3. Spalling characteristics of outburst coal.

the outburst hole will hinder the expansion of the subsequent coal fragments and the throwing out of the coal, which will make the direction of the spalling gradually tends to be perpendicular to the direction of the outburst. The coal and gas outburst is accompanied by a strong dynamic phenomenon, the coal failure in this process turns from strong to weak, resulting in the change of the outburst hole from gradually expanding to gradually narrowing.

The evolution characteristics of the spalling structure of coal in the outburst hole are illustrated in Fig. 3. It can be observed that the coal in the rear section of the outburst hole is damaged, exhibiting a significant spalling phenomenon. At this stage, the direction of spalling is predominantly perpendicular to the direction of the outburst, indicating typical tensile failure characteristics. As the advancing distance increases, the direction of spalling begins to shift upon entering the front section of the outburst hole; this phenomenon is particularly evident near the outburst outlet. The direction of spalling gradually forms an acute angle with the outburst direction, displaying a hemispherical distribution morphology. This can be explained by the principle of the "spherical shell instability" hypothesis: when the outburst outlet is rapidly opened, in-situ stress causes the principal stress in the nearby coal seam to be distributed in a hemispherical shape, concurrently generating Type I cracks of a similar morphology. Under the influence of gas pressure, the tips of these cracks gradually expand, ultimately forming the shape of a spherical crown. After the initiation of the outburst, the coal in close proximity to the outlet is peeled off and ejected along the spherical crown cracks. As the outburst continues and energy is gradually released, the intensity of the outburst weakens. Simultaneously, numerous broken coal fragments left in the outburst hole obstruct the expansion of subsequent coal fragments and their ejection, causing the spalling direction to increasingly align perpendicular to the outburst direction. The coal and gas outburst is characterized by strong dynamic phenomena, with the coal failure transitioning from intense to mild, resulting in the transformation of the outburst hole from gradually expanding to gradually narrowing.

Evolution of pore structure in outburst coal at different excavation distances

Results of low-temperature liquid nitrogen adsorption and pore characteristics

The coal samples used for determining the pore structure were obtained through equidistant excavation and processing. A low-temperature liquid nitrogen adsorption test was conducted on the samples, and the corresponding isothermal adsorption curves were plotted based on the test data, as shown in Fig. 4.

From Fig. 4, it is evident that the adsorption quantity of the coal samples shows an increasing trend with the excavation distance. Combined with Fig. 2, this indicates that the degree of fragmentation of the coal samples closer to the outburst outlet is higher, which increases the gas adsorption space within the samples. Additionally, the adsorption–desorption isothermal curves of the coal samples were analyzed and found to have similar morphologies, conforming to type IV behavior[43]. The desorption curves were consistently above the adsorption curves, with only a slight difference when $p/p_0 < 0.55$. However, the difference became significantly larger when $p/p_0 > 0.5$, and the adsorption and desorption curves did not overlap, exhibiting a hysteresis phenomenon. This behavior indicates the presence of more slit-like and open pores within the samples. Following the adsorption of N_2, micropore filling, single/multiple molecular layer adsorption, and capillary condensation occurred on the pore surfaces, resulting in adsorption and expansion effects.

Based on the low-temperature liquid nitrogen isothermal adsorption curve, the pore size distribution and specific surface area of the pores can be determined by combining various analytical models. Among these, the BJH model is particularly suitable for analyzing the pore size distribution of micropores and some mesopores. However, this model exhibits significant deviation when characterizing pores smaller than 10 nm, whereas the DFT model effectively characterizes pores below 30 nm. Therefore, in this paper, the DFT model (< 10 nm) was utilized in conjunction with the BJH model (> 10 nm) to analyze the adsorption–desorption curves, resulting in the pore size distribution characteristics of coal samples at different excavation distances, as shown in Fig. 5.

Figure 5(a), derived from the DFT model, illustrates that within the test aperture range of less than 10 nm, a pronounced single-peak phenomenon occurs for coal samples at pore sizes of approximately 1.5 nm and 3.0 nm. Additionally, in the pore size range of 3.0 to 4.5 nm, an evident peak area is observed, except for coal samples at excavation distances of 1300–1400 mm and 1400–1500 mm, which either exhibit a dV of 0 $cm^3/nm/g$ or only a small peak area. This pattern is consistent with the findings reported in reference[36]. The pore size range of 4.5 to 10.0 nm reveals the presence of single or multiple peaks at each excavation distance. As the excavation

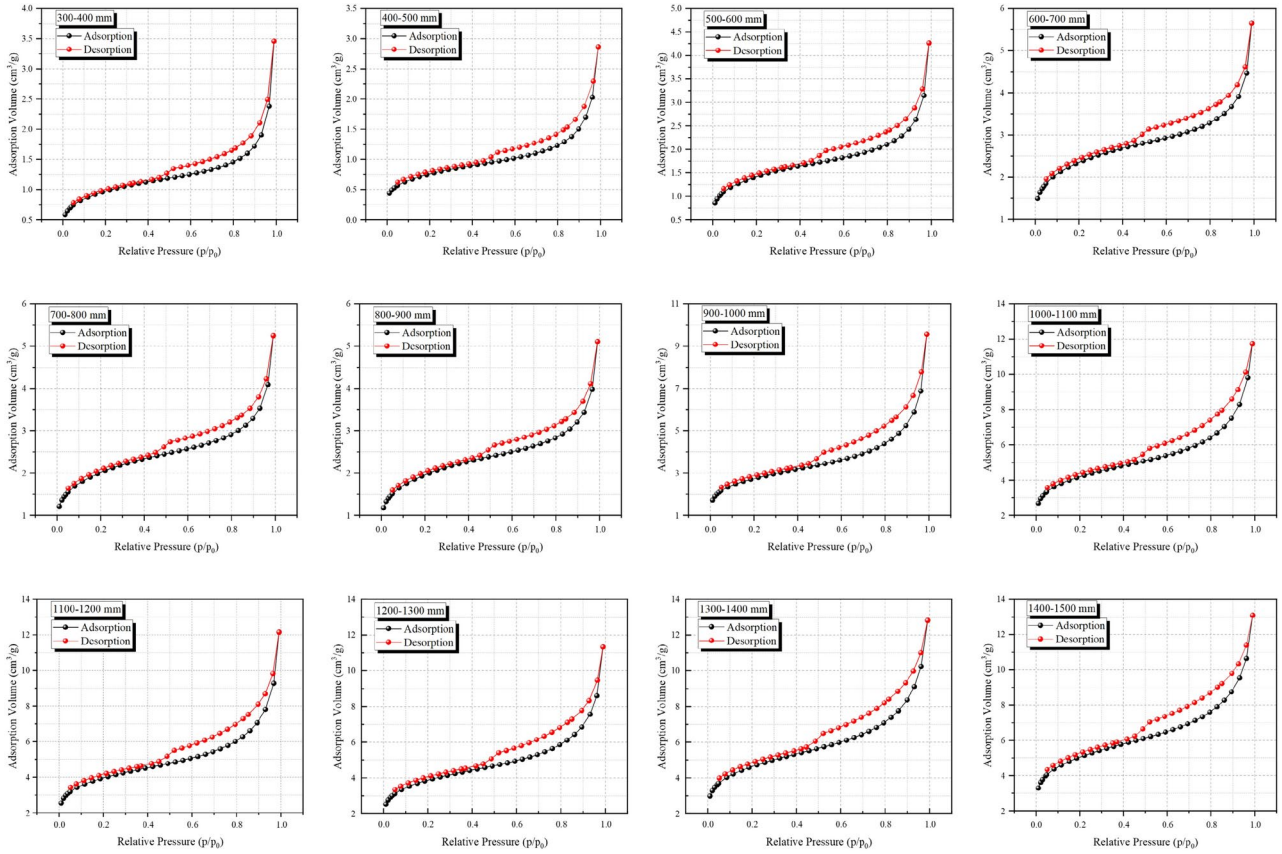

Fig. 4. The low-temperature liquid nitrogen isothermal adsorption curves of coal samples.

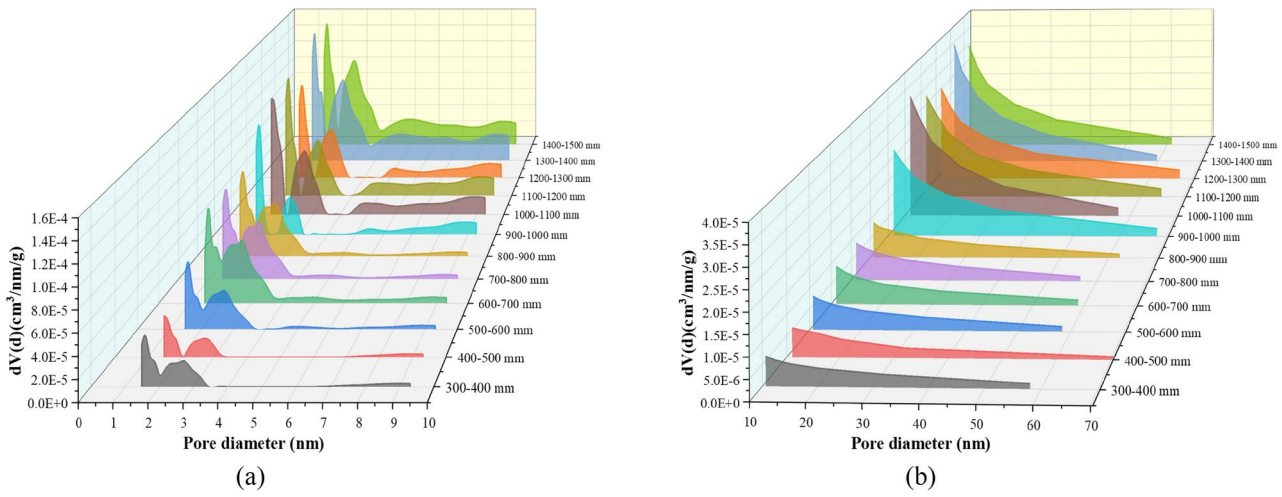

Fig. 5. Pore size distribution of coal samples with varying excavation distances.

distance increases, both the number of peaks and the peak area gradually increase, particularly notable between excavation distances of 900 mm and 1500 mm. The size of the peak area corresponds to the dV value, which characterizes the pore volume in the samples, indicating that the pores are more developed in the size ranges where peaks occur.

Figure 5(b), derived from the BJH model, indicates that the pore size distribution characteristics across each excavation distance exhibit certain similarities, all demonstrating a decreasing trend with increasing pore size. The maximum pore volume peaks at a pore size of 10 nm. Within the excavation distance of 300–900 mm, the maximum pore volume fluctuates but remains relatively stable. However, beyond an excavation distance of 900 mm, the maximum pore volume increases in a stepwise manner, fluctuating within the range

of 900–1500 mm, and is significantly higher than the maximum pore volume observed in the 300–900 mm range. This suggests that the mesopore and macropore volumes of the coal samples at excavation distances greater than 900 mm are considerably larger than in other ranges. This phenomenon may be attributed to the substantial energy accumulated within the coal during the outburst, where the coal near the outburst outlet was first destroyed and expelled, intensifying the destruction and promoting internal pore development. As the outburst continued and energy was gradually released, the degree of destruction in the middle and rear coal seams diminished, leading to a reduction in pore development. It is speculated that a mutation of energy during this process caused the observed step change in pore volume.

To quantify the differences in pore structure among coal samples at varying excavation distances, the pore volume and specific surface area of the samples within the excavation range were determined based on the analytical results from the DFT, BJH, and BET models. The statistical findings are summarized in Table 1.

As shown in Table 1, significant variations in pore volume and specific surface area were observed in coal samples across different excavation distances. The total pore volume within the coal seam excavation distances ranged from 0.454×10^{-2} cm^3/g to 2.266×10^{-2} cm^3/g, with an extreme difference of 1.813×10^{-2} cm^3/g, while the specific surface area ranged from 2.626 m^2/g to 16.697 m^2/g, showing an extreme difference of 14.071 m^2/g. Further analysis within the 300–1500 mm excavation distance range revealed that the maximum micropore volume was 0.435×10^{-2} cm^3/g, and the minimum was 0.048×10^{-2} cm^3/g, with a difference of 0.387×10^{-2} cm^3/g. Similarly, the mesopore volume difference was 1.518×10^{-2} cm^3/g, and the macropore volume difference was 0.233×10^{-2} cm^3/g. Compared to the macropore volume, the micropore and mesopore volumes were larger by factors of 1.661 and 6.515, respectively. These results indicate that differences in the pore structure of coal samples at various excavation distances primarily manifest in the micropore and mesopore volumes, which substantially increase specific surface area. This suggests that as an outburst develops, coal samples closer to the outburst surface undergo more intense crushing, leading to greater gas storage space and a higher adsorption capacity.

Fractal characteristics

To describe the complexity and irregularity of the internal pore structure of the coal, the fractal dimension D was introduced to characterize it, and the larger the value of D. A higher D value indicates a rougher material surface and a more intricate pore structure. The low-temperature liquid nitrogen adsorption results were analyzed using the Frenkel-Halset-Hill (FHH) model, which enabled the calculation of the adsorption pore fractal dimension D[44]. The results can be obtained from Eq. (1) to Eq. (2).

$$ln\left(\frac{V}{V_0}\right) = n + mln\left[ln\left(\frac{p_0}{p}\right)\right] \tag{1}$$

$$D = m + 3 \tag{2}$$

where: V was the gas adsorption volume at the equilibrium pressure p, cm^3/g; V_0 was the monolayer adsorption volume, cm^3/g; p_0 was the saturation vapor pressure of the gas, kPa; p was the pressure at which the gas adsorption reached the equilibrium, kPa; m was the slope of the fitted straight line; and n was the fitting constant.

The desorption stage in the low-temperature liquid nitrogen isothermal adsorption curve was utilized to determine the fractal dimension, with the fractal dimension characteristics of coal samples at varying excavation distances presented in Fig. 6.

Due to variations in the adsorption mechanisms of coal samples for gas across different pressure ranges, analysis of the adsorption–desorption curves reveals that the fractal dimension data can be divided into two

Excavation distance(mm)	Pore volume($\times 10^{-2}$ cm^3/g)				BET specific area(m^2/g)
	Micropore	Mesopore	Macropores	Toal	
300 ~ 400	0.073	0.316	0.169	0.558	3.287
400 ~ 500	0.048	0.019	0.387	0.454	2.626
500 ~ 600	0.110	0.417	0.170	0.698	4.793
600 ~ 700	0.209	0.568	0.180	0.957	7.836
700 ~ 800	0.164	0.538	0.178	0.880	6.805
800 ~ 900	0.160	0.523	0.174	0.856	6.622
900 ~ 1000	0.199	0.955	0.306	1.460	9.174
1000 ~ 1100	0.337	1.293	0.283	1.913	13.917
1100 ~ 1200	0.330	1.252	0.402	1.983	13.092
1200 ~ 1300	0.313	1.180	0.319	1.813	12.800
1300 ~ 1400	0.398	1.521	0.314	2.233	15.346
1400 ~ 1500	0.435	1.537	0.294	2.266	16.697

Table 1. Results of nitrogen adsorption tests.

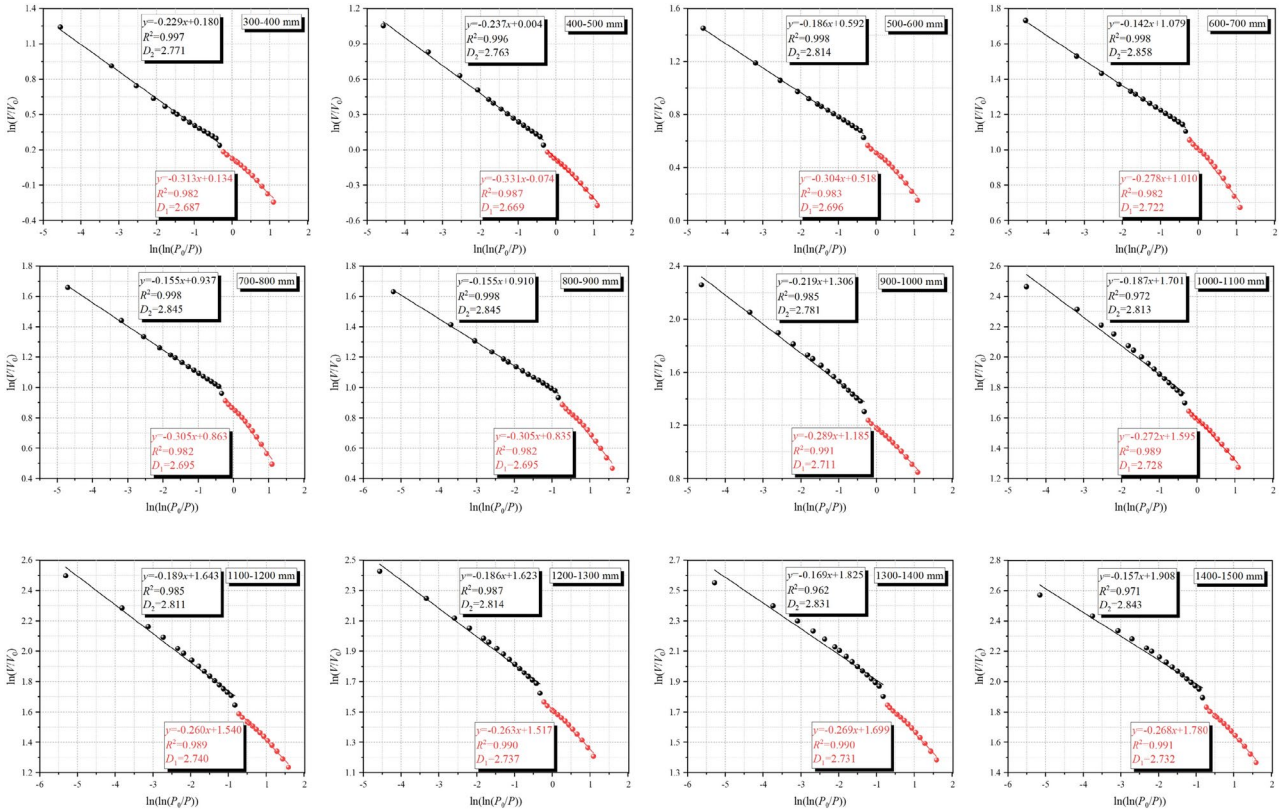

Fig. 6. Fractal dimension characteristics of nitrogen adsorption pore sizes in coal samples at different excavation distances.

Excavation distance(mm)	D_1	R^2	D_2	R^2
300 ~ 400	2.687	0.982	2.771	0.997
400 ~ 500	2.669	0.987	2.763	0.996
500 ~ 600	2.696	0.983	2.814	0.998
600 ~ 700	2.722	0.982	2.858	0.998
700 ~ 800	2.695	0.982	2.845	0.998
800 ~ 900	2.695	0.982	2.845	0.998
900 ~ 1000	2.711	0.991	2.781	0.985
1000 ~ 1100	2.728	0.989	2.813	0.972
1100 ~ 1200	2.740	0.989	2.811	0.985
1200 ~ 1300	2.737	0.990	2.814	0.987
1300 ~ 1400	2.731	0.990	2.831	0.962
1400 ~ 1500	2.732	0.991	2.843	0.971

Table 2. Calculation results of fractal dimension.

phases: low-pressure and high-pressure at $\ln(p_0/p) = 0.5$. The data from each phase were linearly fitted to obtain fractal dimensions D_1 and D_2, with the summarized results presented in Table 2.

As shown in Table 2, the R^2 values of each fitted line exceed 0.980, indicating a high goodness of fit. With increasing excavation distance, D_1 rises from 2.669 to 2.740, with a maximum deviation of 0.071, showing an overall upward trend. This suggests that coal samples nearer to the outburst outlet have rougher pore surfaces, and their internal structure becomes progressively more complex. Meanwhile, D_2 varies from 2.763 to 2.858, with a maximum deviation of 0.095, showing fluctuations that indicate the pore fractal characteristics of the coal are affected differently by distance from the outburst surface during the outburst process. Additionally, D_2 is consistently larger than D_1 at each excavation distance, suggesting that the coal's pore structure in the high-pressure phase is more complex, irregular, and heterogeneous.

Gas adsorption characteristics of outburst coal at varying excavation distances

High-pressure gas adsorption tests were conducted on coal samples at different excavation distances. Simultaneously, the Langmuir equation model (Eq. 3) was employed to fit the test data[45], establishing the relationship between gas adsorption and pressure. This process allowed for the generation of isothermal adsorption curves for CH_4, as shown in Fig. 7. The model expression is as follows:

$$Q=\frac{ahp}{1+hp} \tag{3}$$

where Q is the amount of gas adsorbed from coal samples at a certain temperature and pressure, mL; p is the adsorption equilibrium pressure, MPa; a is the adsorption constant, which indicates the limit of the adsorbed gas amount of coal samples at a certain gas pressure, mL/g; and h is the adsorption constant, MPa^{-1}.

Figure 7 illustrates that the isothermal adsorption curves of coal samples at different excavation distances exhibit similar morphology. Due to the positive effects of pressure adsorption, the amount of gas adsorption gradually increases with rising adsorption pressure and ultimately stabilizes. The data presented in the figure are summarized in Table 3.

Table 3 indicates that the goodness of fit for each isothermal adsorption curve exceeds 0.990. The gas adsorption capacity of coal samples increases from 10.140 cm^3/g to 18.987 cm^3/g with greater excavation distance, resulting in a maximum difference of 8.847 cm^3/g, which represents an increase of 87.249%. Notably, the gas adsorption quantity for coal samples at excavation distances between 900 and 1000 mm shows a sudden increase, indicating that closer proximity to the outburst correlates with higher adsorption capacity. This relationship is attributed to the more severe destruction of coal on the outburst side, leading to increased fragmentation. Furthermore, as analyzed in the previous section regarding pore size distribution, the outburst process alters the pore structure of coal samples. As excavation distance increases, there is a significant rise in both micropores and mesopores, while the increase in pore volume and specific surface area offers richer adsorption space for gas. Consequently, pore size distribution and gas adsorption quantity are correlated, exhibiting a similar pattern of change.

The gas adsorption constant of coal is a critical index for measuring gas adsorption capacity and serves as a key parameter for the ultimate adsorption amount and pressure sensitivity under varying pressures. The adsorption constant values of coal samples at different excavation distances range from 13.227 ml/g to 23.564 ml/g. The observed trend of gradual increase with excavation distance indicates that coal samples closer

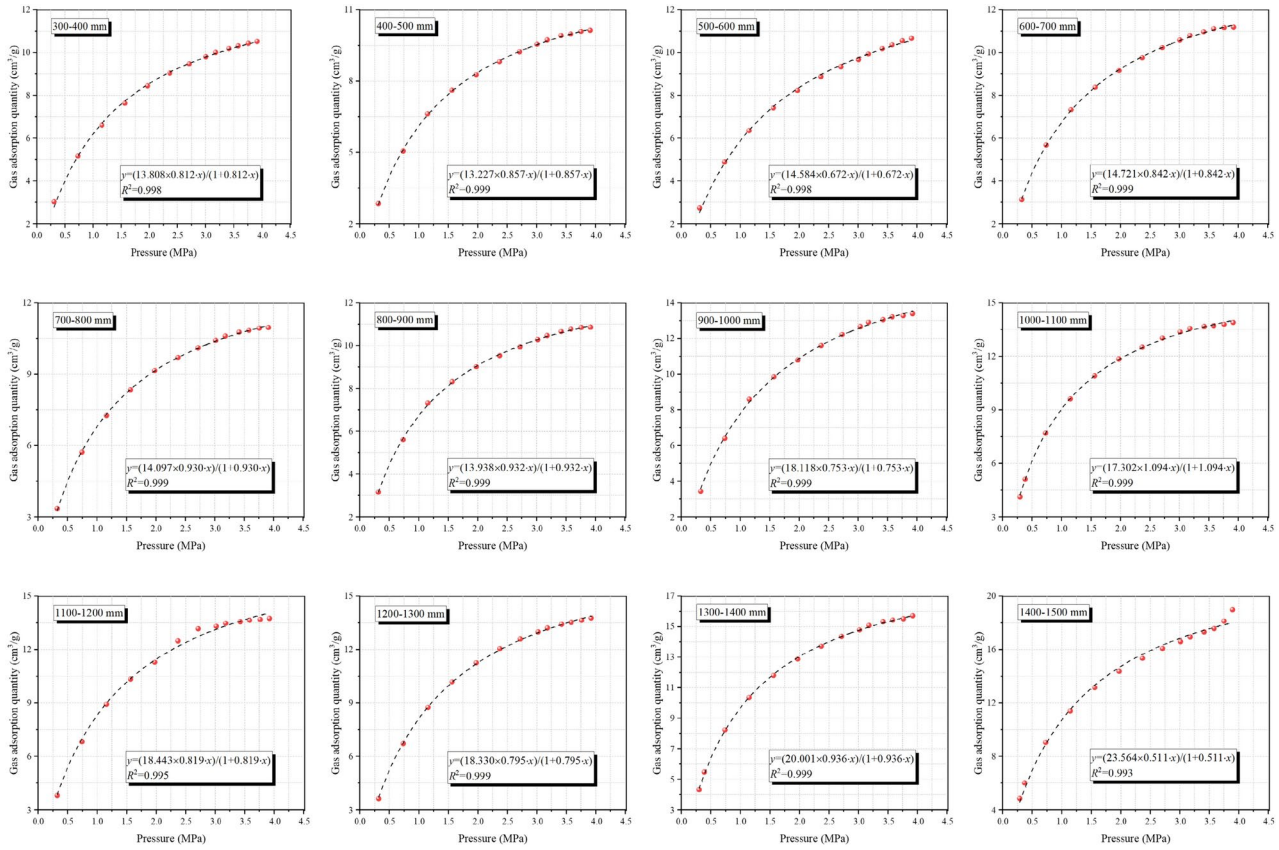

Fig. 7. Isothermal adsorption curves of CH_4 for coal samples at varying excavation distances.

Excavation distance(mm)	Q (cm^3/g)	a (ml/g)	b (MPa^{-1})	R^2
300 ~ 400	10.514	13.808	0.812	0.998
400 ~ 500	10.140	13.227	0.857	0.999
500 ~ 600	10.658	14.584	0.672	0.998
600 ~ 700	11.190	14.721	0.842	0.999
700 ~ 800	10.967	14.097	0.930	0.999
800 ~ 900	10.866	13.938	0.932	0.999
900 ~ 1000	13.405	18.118	0.753	0.999
1000 ~ 1100	13.903	17.302	1.094	0.999
1100 ~ 1200	13.743	18.443	0.819	0.995
1200 ~ 1300	13.766	18.330	0.795	0.999
1300 ~ 1400	15.718	20.001	0.936	0.999
1400 ~ 1500	18.987	23.564	0.511	0.993

Table 3. Adsorption parameters of coal samples.

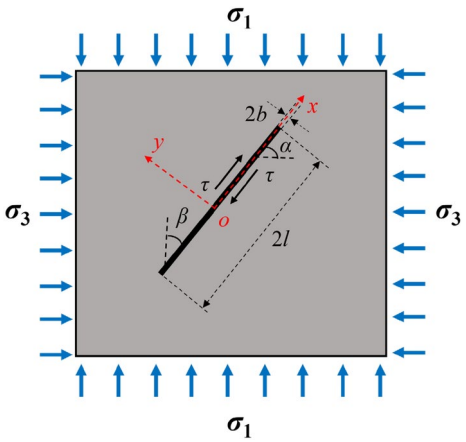

Fig. 8. The stress state of closed fracture under initial ground.

to the outburst outlet exhibit higher ultimate adsorption quantities. Additionally, the bb values fluctuate within the range of 0.511 to 1.904 MPa^{-1}, suggesting that coal samples at different excavation distances respond more rapidly to changes in gas pressure.

Discussion

Coal and gas outburst is a complex dynamic disaster in underground coal mines, and accurately characterizing the mechanism behind their occurrence is challenging. Additionally, due to the spatial constraints and instantaneous nature of outbursts, only limited information can be gathered regarding this process; however, this information is crucial for studying the outburst mechanism. The pore size distribution of coal, along with its adsorption and desorption properties during coal and gas outbursts, plays a significant role in understanding the development mechanism of such events. Therefore, investigating the mechanism of coal and gas outbursts at the microscopic level by analyzing pore size changes and the adsorption and desorption properties of coal samples, in conjunction with fracture mechanics, is a scientifically sound and effective approach.

Analysis of fracture mechanics state of coupled coal seam to be mined in far-field

During the mining process, the coal seam to be mined in the far-field is in the state of coupled equilibrium between the stress field and the gas field, that is to say, the coal is in the three-direction stress equalization, and the gas field is in the relative stationary state. To analyze the microscopic mechanical properties of the coal seam in this coupled state, a unit body containing a primary crack (assumed to be in a closed state, with a length of 2 l and a width of 2b) is considered. Given the closure of the crack, it is assumed that $b/l < 0.2$, allowing calculations based on the scenario of an infinite plate with a closed crack[46].

Based on the theory of fracture mechanics[47] (noting that this paper does not address the wing crack initiation angle solution, and thus does not analyze the influence of T stress on the fracture mechanism of rock compression shear cracks in depth), a coordinate system is established with the long axis aligned along the x-direction and the short axis along the y-direction, with their intersection serving as the origin. The far-field stress state is then analyzed, and the stress state of closed fracture under initial ground as shown in Fig. 8.

$$\left.\begin{aligned}\sigma_x &= \sigma_1 \cos^2\beta + \sigma_3 \sin^2\beta \\ \sigma_y &= \sigma_1 \sin^2\beta + \sigma_3 \cos^2\beta \\ \tau &= (\sigma_1 - \sigma_3)\sin\beta\cos\beta\end{aligned}\right\} \tag{4}$$

where σ_1 and σ_3 are the vertical and horizontal in-situ stresses, MPa; σ_x and σ_y are the stresses in the x and y directions, MPa; τ is the shear stress in the x direction, MPa; β is the angle between the direction of the long axis of the crack and the vertical stress.

At this stage, the rock mass above and below the crack face exhibits a tendency for relative slip, generating friction that resists this sliding. Consequently, the far-field shear stress acting on the closed crack is denoted as $\tau_m = \tau$, while the normal stress is represented as $\sigma_n = \sigma_y$. The equivalent shear stress can then be expressed as follows[48]:

$$\tau_e = \tau_m - \tau^f \tag{5}$$

In addition, the equivalent friction $\overline{\tau}$ is introduced, which is the average of $\tau^f(x)$ in the sense of an integral over the entire crack surface:

$$\overline{\tau} = \tau_0 + f\sigma_n = \tau_0 + f\left(\sigma_1 \sin^2\beta + \sigma_3 \cos^2\beta\right) \tag{6}$$

where f is the friction coefficient between the cracks.

The equivalent shear stress is:

$$\tau_e = \tau - \overline{\tau} = \tau - \tau_0 - f\sigma_y \tag{7}$$

This can be obtained by bringing Eq. (4) into Eq. (7):

$$\tau_e = \frac{\sigma_1 - \sigma_3}{2}\sin 2\beta - f\left(\sigma_1 \sin^2\beta + \sigma_3 \cos^2\beta\right) - \tau_0 \tag{8}$$

Therefore, the stress intensity factor at the crack tip induced by the far-field stress is given by[49]:

$$K_{\mathrm{II}} = \tau_e\sqrt{\pi l} \tag{9}$$

This can be obtained by bringing Eq. (8) into Eq. (9):

$$K_{\mathrm{II}} = \left[\frac{\sigma_1 - \sigma_3}{2}\sin 2\beta - f\left(\sigma_1 \sin^2\beta + \sigma_3 \cos^2\beta\right) - \tau_0\right]\sqrt{\pi l} \tag{10}$$

At this time, the fracture toughness corresponding to mode II fracture is:

$$k_{\mathrm{IIc}} = (\sigma_{1c} - \sigma_3)\sqrt{\pi l} \tag{11}$$

Under critical conditions are:

$$|K_{\mathrm{II}}| = K_{\mathrm{IIc}} \tag{12}$$

$$k_{\mathrm{IIc}} = \frac{2\left[K_{\mathrm{IIc}} + (\tau_0 + f\sigma_3)\sqrt{\pi l}\right]}{\sin 2\beta - f\left(1 - \cos 2\beta\right)} \tag{13}$$

From Eq. (13), the fracture toughness is related to the confining pressure σ_3 and the angle β. Furthermore, due to the balance of gas pressure inside and outside the closed crack in the coal, this crack can be treated as a Griffith crack. Therefore, considering the deterioration effect of the adsorbed gas at the crack tip, it follows that the impact of the adsorbed gas on the crack can be expressed using Griffith's formula[50]. The tensile stress σ_t produced by the adsorbed gas inside the crack is:

$$\sigma_t = \sqrt{\frac{2E\gamma'}{\pi l}} \tag{14}$$

where γ' is the surface free energy of adsorbed gas, N/m; E is the elastic modulus of coal, Pa; l is the length of crack, m.

Where γ' is calculated as follows:

$$\gamma' = \gamma_0 - \frac{RT}{V_0 S_0}\int_0^p \frac{V_p}{p}\mathrm{d}p \tag{15}$$

This can be obtained by bringing Eq. (12) into Eq. (11):

$$\sigma_t = \left[\frac{2E}{\pi l}\left(\gamma_0 - \frac{\mathrm{RT}}{S_0 \mathrm{V}_0}\int_0^p \frac{V_p}{p}\mathrm{d}p\right)\right]^{\frac{1}{2}} \tag{16}$$

where γ_0 is the surface free energy of adsorbed gas under vacuum, N/m; R is the gas constant, taken as 8.314 3 J/(mol·K); T is the kelvin temperature, K; V_0 is the molar volume, 22.4 × 10 L/mol; S_0 is the specific surface area of coal, m^2/g; V_p is the amount of adsorbed gas content of the coal at adsorption equilibrium, m^3/t.

From the above equation, the adsorbed gas induces irreversible expansion and deformation of the coal, resulting in a decrease in the surface free energy of the coal, which subsequently reduces the tensile strength at the crack tips. In summary, it is evident that the cracks present in the coal seam to be mined in the far-field are simultaneously subjected to the pressure-shear effect from in-situ stress and the deterioration caused by the adsorbed gas.

Analysis of the gas–solid coupling mechanism in coal instability

The in-situ stress of coal in front of the outburst outlet, caused by rapid unloading, results in stress concentration due to the dynamic stress field, affecting the coal. According to the stress concentration coefficient derived from the literature[51], the maximum stress on the coal in front of the outburst outlet is 2 to 3 times the initial stress. Consequently, a non-uniform stress field is generated within the coal under the influence of high stress. Figure 9 illustrates the distribution of stress in the coal near the exposed surface under disturbance.

Existing theory[52] suggests that roadway excavation causes stress redistribution in the coal ahead and classifies the stress states into three areas: the initial stress area (I), the stress concentration area (II), and the pressure relief area (III). In the stress concentration area, plastic failure occurs in the coal, leading to the opening of cracks, an increase in pore content, and a portion of the adsorbed gas transitioning to a free state (assuming that the pressure of the free gas after desorption is P_1).

The morphology and mechanical state of the internal cracks change when the studied unit transitions from the initial stress area to the stress concentration area. In conjunction with the literature[53], a comprehensive model of cracks under the coupling of stress and gas fields is developed, as illustrated in Fig. 10.

The internal cracks in the coal transition from initial closure to opening. The open-type cracks are influenced not only by the far-field stress but also by the expansion stress of the internal free gas and the tensile stress generated at the tips of the cracks. Therefore, if the cracks continue to expand, the coal is compromised, resulting in the formation of I-II composite failure cracks[54].

According to the principle of stress superposition, the crack state is analyzed by stress[55], as shown in Fig. 11. Here, τ_t represents the shear stress in the short-axis direction of the fracture[56], and it is considered negligible due to its small magnitude.

The stress intensity factor caused by far-field stress is:

$$\begin{cases} K_{\mathrm{I-s}} = \sigma_y\sqrt{\pi l} = \left(\sigma_1 \sin^2\beta + \sigma_3 \cos^2\beta\right)\sqrt{\pi l} \\ K_{\mathrm{II}} = \tau_e\sqrt{\pi l} \end{cases} \tag{17}$$

where: $K_{I\text{-}s}$ is the far-field stress component of K_I.

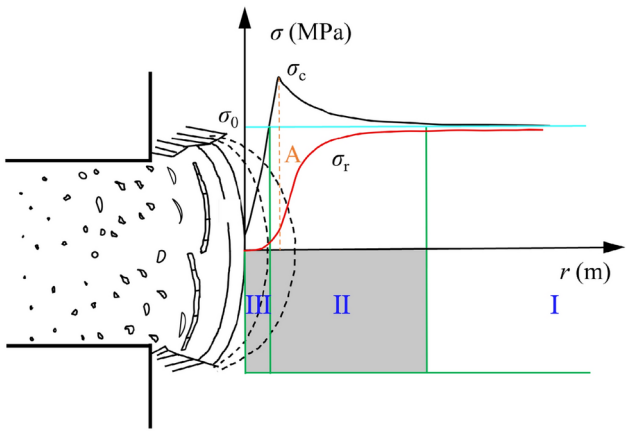

Fig. 9. Stress distribution in the coal at the front of the exposed surface.

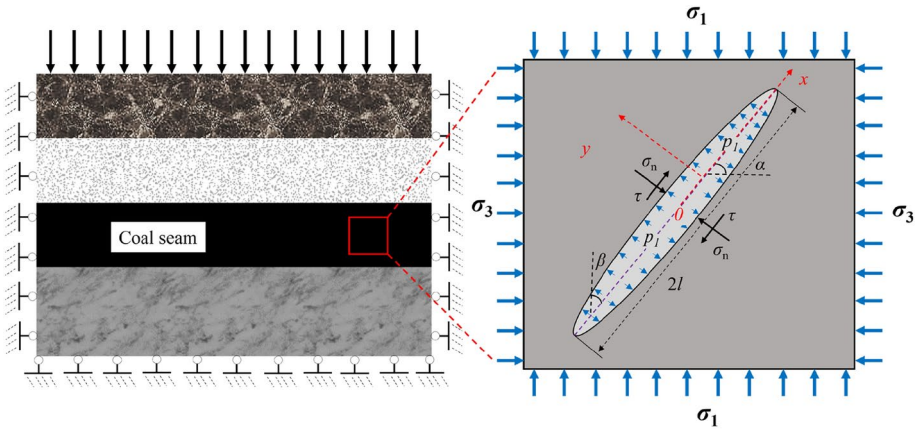

Fig. 10. Fracture model under the coupling effect of the stress field and gas field.

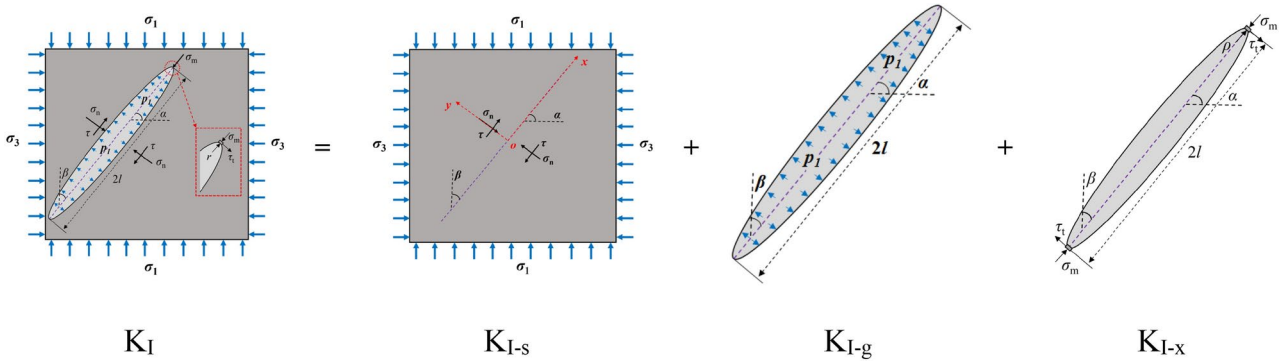

Fig. 11. Stress state of gas-containing open fracture.

The stress intensity factor induced by the expansion pressure of free gas is given by:

$$K_{\mathrm{I-g}} = \frac{p_1}{2l}\sqrt{\pi l} \tag{18}$$

According to the conclusion drawn by Muskhelishvili N.I.[57], for elliptical cracks with long and short axes of 2 l and 2b, respectively, the compressive stress applied at their tips generates a tensile stress that is perpendicular to the compressive stress and equal in magnitude. Therefore, the stress intensity factor due to this tensile stress is:

$$K_{\mathrm{I-x}} = 0.5\sigma_x\sqrt{\rho/l}\sqrt{\pi l} \tag{19}$$

where ρ is the radius of curvature of the crack tip and $\rho \to 0$.

Therefore, the type I stress intensity factor of the open cracks under the action of stress and gas field is:

$$K_{\mathrm{I}} = K_{\mathrm{I-s}} + K_{\mathrm{I-g}} + K_{\mathrm{I-x}} = \left[\left(\sigma_1 \sin^2\beta + \sigma_3\cos^2\beta\right) + \frac{p_1}{2l} + 0.5\sigma_x\sqrt{\rho/l}\right]\sqrt{\pi l} \tag{20}$$

After being disturbed by mining, the cover rock load is transferred, disrupting the equilibrium state of the coal with a tendency for outburst. At this point, the coal experiences sudden unloading, causing the in-situ stress near the exposed surface to resemble a unidirectional state. Taking the location of the maximum in-situ stress illustrated in Fig. 9 as an example, which is situated at the front of the exposed surface, the axial stress increases while the circumferential stress gradually decreases, approaching zero. The mechanical changes are depicted in Fig. 12.

By combining Eq. (17) to analyze the stress state of the open crack, the stress intensity factor at this point can be expressed as:

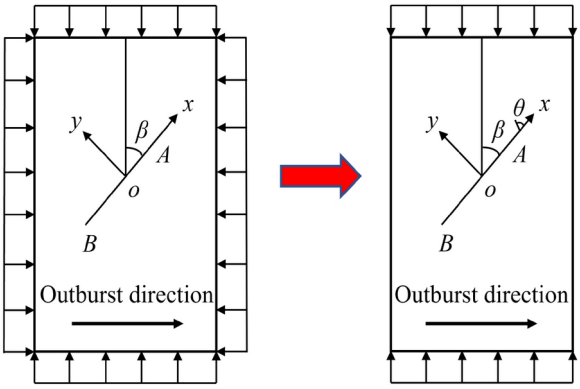

Fig. 12. Changes in the mechanical state of coal seams before and after an outburst.

$$\begin{cases} K_{\mathrm{I}} = \left(\sigma_1 \sin^2\beta + \dfrac{p_1}{2l} + 0.5\sigma_1 \cos^2\beta\sqrt{\rho/l}\right)\sqrt{\pi l} \\ K_{\mathrm{II}} = \left[\sigma_1 \sin\beta\left(\cos\beta - f\sin\beta\right) - \tau_0\right]\sqrt{\pi l} \end{cases} \tag{21}$$

Noting that the critical load is σ'_1, the uniaxial compressive brittle fracture ability of crack coal is:

$$k'_{\mathrm{IIc}} = \sigma'_{1c}\sqrt{\pi l} \tag{22}$$

Combining the theory of fracture mechanics, the expression for σ_θ near the crack tip can be obtained as follows:

$$\sigma_\theta = \frac{-3K_{\mathrm{II}}}{2\sqrt{2\pi r}} \cos\frac{\theta}{2}\sin\theta \tag{23}$$

where θ is the angle between the tangent to the crack propagation path at the initial breaking point aa and the crack direction (x-axis) (Fig. 12).

It is worth noting that both θ and r in Eqs. (20) and (21) are expressed in polar coordinates[58], leading to the following conclusion:

$$k'_{\mathrm{IIc}} = \frac{2\left(K_{\mathrm{IIc}} + \tau_0\sqrt{\pi l}\right)}{\sin 2\beta - f\left(1 - \cos 2\beta\right)} \tag{24}$$

By comparing Eqs. (10), (13), (21), and (24), it is evident that the type II stress intensity factor increases while the brittle fracture resistance decreases in a unidirectional stress state, making the internal cracks in the coal more susceptible to expansion. Furthermore, the tensile stress within the cracks exacerbates the destruction process of the coal.

In this state, the internal cracks of the coal will be influenced by the combined effects of type I and type II stress intensity factors, leading to the formation of composite cracks at the tips. Under high stress, the cracks within the coal will expand and propagate from the tips, gradually forming vertical cracks[59–61].

The cracks that form under high stress during stress concentration propagate toward the direction of maximum principal stress, resulting in the development of vertical cracks. Plastic failure disrupts the gas pressure equilibrium within the coal, causing some of the gas to transition from an adsorbed state to a free state, with the gas pressure in the free state changing from P_0 at the initial time to P_1. Additionally, as the outburst continues, the coal at the exposed surface is stripped away and displaced, leading to a gradual reduction in the axial stress of the coal and the formation of a new exposed surface. Consequently, the coal primarily experiences gas pressure from within, further expanding the cracks created by plastic failure, and the crack tips are subjected to tensile stress due to their sharp tendency to open.

The expressions for the effective transverse compressive stress σ'_1 and the effective normal compressive stress σ'_n under the influence of free gas, as provided in[53], are as follows:

$$\begin{cases} \sigma'_1 = \dfrac{(\sigma_1 + \sigma_3) - (\sigma_1 - \sigma_3)\cos 2\alpha}{2} - p_1 \\ \sigma'_n = \dfrac{(\sigma_1 + \sigma_3) + (\sigma_1 - \sigma_3)\cos 2\alpha}{2} - p_1 \end{cases} \tag{25}$$

This can be obtained by substituting $\sigma_3 = 0$ MPa and $\alpha = 90°$ into the above equation:

$$\begin{cases} \sigma'_1 = \sigma_1 - p_1 \\ \sigma'_n = -p_1 \end{cases} \tag{26}$$

Then, the type I stress intensity factor generated at the crack tip is:

$$K_I = \sqrt{\pi l}\left(p_1 + \sigma_1\sqrt{\frac{\rho}{l}}\right) \tag{27}$$

For the coal at the exposed surface, the axial stress on the cracks was already low, and the rise in internal free gas pressure became the primary factor driving the continued expansion of the cracks. Under the influence of gas, the coal continues to be crushed and pulverized, resulting in a further increase in its internal pore volume and a gradual complexity in its pore structure.

Under the influence of high in-situ stress acting on the coal in front of the exposure, the stress intensity factor at the tip of the internal original crack exceeds the resistance to brittle fracture, leading to the propagation of macroscopic cracks. This, in turn, results in the plastic failure of the coal and the desorption of internal adsorbed gas, altering its state of occurrence and allowing stress to dominate the outburst process. As the outburst progresses, stress redistribution at the newly exposed surface approximates a unidirectional compression state. With the continuous reduction of axial stress, the free gas pressure inside the crack increases, enhancing the tensile stress intensity factor at the crack tip, which causes further crack propagation. At this stage, the tensile effect generated by gas pressure plays a crucial role in the outburst process. When the deformation and destruction of coal reach a critical state, the coal is torn, crushed, and expelled under the combined influence of elastic potential energy and gas internal energy, resulting in a noticeable spalling phenomenon. This phenomenon further corroborates that coal and gas outbursts are the result of the combined actions of in-situ stress, gas pressure, and the physical properties of coal.

Conclusions

In this study, a large-scale coal and gas outburst test was conducted, followed by the excavation and sampling of protruding coal at fixed distances. The obtained coal samples were processed through grinding and sieving. The pore structure characteristics and gas adsorption properties of the coal samples were analyzed using pore structure determination and high-pressure gas adsorption tests at each excavation distance. Ultimately, the study investigated the mechanism of coal disasters caused by the interplay of deteriorating in-situ stress and gas pressure, in conjunction with fracture mechanics theory, at the microscopic level. The main conclusions are as follows:

1. The outburst hole formed after the termination of the coal and gas outburst, displaying an approximately symmetrical distribution along the center line of the outburst outlet in a "V" shape. This morphology is characterized by a small mouth and large cavity in the front section, transitioning to a large mouth and small cavity in the rear section. Additionally, there were notable spalling phenomena on the surface of the hole, which was spherical at the outlet, while the remaining sections exhibited a vertical distribution.
2. The morphology of the low-temperature liquid nitrogen isothermal adsorption curves for the coal samples was similar, and all of them exhibiting an adsorption hysteresis phenomenon. The specific surface area and pore volume showed a positive correlation with excavation distance, where the specific surface area increased from 2.626 m^2/g to 16.697 m^2/g and the total pore volume increased from 0.454×10^{-2} cm^3/g to 2.266×10^{-2} cm^3/g as the excavation distance ranged from 100 to 1300 mm. Notably, the difference in pore volume for micropores and mesopores was 6.515 times and 1.661 times greater than that for macropores, respectively, indicating that the variation in pore structure is primarily observed in the micropores and mesopores. Additionally, with increasing excavation distance, the fractal dimension D_1 changed from 2.669 to 2.740, showing a general upward trend, while D_2 fluctuated between 2.763 and 2.858. This suggests that the pore structure of the coal in the high-pressure stage became more complex and irregular, resulting in increased heterogeneity.
3. The gas isothermal adsorption curves for the coal samples exhibited similar morphology, with gas adsorption quantity gradually increasing with rising adsorption pressure until reaching a stable level. As excavation distance increased, the gas adsorption quantity of the coal samples increased, and the value of adsorption constant *a* increased, which ranged from 13.227 to 23.564 ml/g. Meanwhile, the adsorption constant *b* fluctuated between 0.511 and 1.904 MPa^{-1}. The relationship between gas adsorption quantity and the pore structure characteristics of the coal samples was consistent, indicating that changes in these two parameters followed a similar trend.
4. Under the combined effects of in-situ stress and gas pressure, the tips of the internal cracks in the coal expand and continue to extend in the direction of the maximum principal stress. The stress state transitions from compressive-shear to tensile-shear and ultimately to tensile stress, resulting in the broken coal being expelled and forming an outburst hole.

Data availability

The datasets used and/or analysed during the current study are available from the corresponding author on reasonable request.

Received: 4 June 2024; Accepted: 19 February 2025
Published online: 02 March 2025

References

1. Yuan, L. Strategic thinking of simultaneous exploitation of coal and gas in deep mining. *J. China Coal Soc.* **41**(1), 1–6 (2016).
2. Yuan, L. Research progress of mining response and disaster prevention and control in deep coal mines. *J. China Coal Soc.* **46**(3), 716–725 (2021).
3. Xu, C. et al. Apparent-depth effects of the dynamic failure of thick hard rock strata on the underlying coal mass during underground mining. *Rock Mech. Rock Eng.* **52**, 1565–1576 (2019).
4. Yang, Y. et al. Influence of soluble organic matter on mechanical properties of coal and occurrence of coal and gas outburst. *Powder Technol.* **332**, 8–17 (2018).
5. Hou, W. et al. Experimental research into the effect of gas pressure, particle size and nozzle area on initial gas-release energy during gas desorption. *Int. J. Mining Sci. Technol.* **31**(2), 253–263 (2021).
6. Gao, D. et al. Experimental study on the deformation behaviour, energy evolution law and failure mechanism of tectonic coal subjected to cyclic loads. *Int. J. Mining Sci. Technol.* **32**(6), 1301–1313 (2022).
7. Alexeev, A. D. et al. True triaxial loading apparatus and its application to coal outburst prediction. *Int. J. Coal Geol.* **58**(4), 245–250 (2004).
8. Sobczyk, J. A comparison of the influence of adsorbed gases on gas stresses leading to coal and gas outburst. *Fuel* **115**, 288–294 (2014).
9. Wang, C. et al. Experimental analysis of the intensity and evolution of coal and gas outbursts. *Fuel* **226**, 252–262 (2018).
10. Peng, S. J. et al. Experimental study on the influence mechanism of gas seepage on coal and gas outburst disaster. *Saf. Sci.* **50**(4), 816–821 (2012).
11. Pan, X. et al. An experimental study of the mechanism of coal and gas outbursts in the tectonic regions. *Eng. Geol.* **279**, 105883 (2020).
12. Zhang, M. et al. Quantitative study on the role of desorption gas on coal-gas outbursts: Energy contribution and dynamic characteristics. *Process Saf. Environ. Protect.* **171**, 437–446 (2023).
13. Yang, W. et al. How in situ stresses and the driving cycle footage affect the gas outburst risk of driving coal mine roadway. *Tunnell. Undergr. Space Technol.* **31**, 139–148 (2012).
14. Lei, Y. et al. Experimental investigation on the mechanism of coal and gas outburst: novel insights on the formation and development of coal spallation. *Rock Mech. Rock Eng.* **54**, 5807–5825 (2021).
15. Cao, J. et al. A novel large-scale three-dimensional apparatus to study mechanisms of coal and gas outburst. *Int. J. Rock Mech. Min. Sci.* **118**, 52–62 (2019).
16. Xue, S. et al. Occurrence and development criteria of coal and gas outbursts based on energy conversion. *Fuel* **341**, 127781 (2023).
17. Wang, H. et al. Analysis of precursor information for coal and gas outbursts induced by roadway tunneling: A simulation test study for the whole process. *Tunnell. Undergr. Space Technol.* **122**, 104349 (2022).
18. Lei, Y. et al. The energy principle of coal and gas outbursts: experimentally evaluating the role of gas desorption. *Rock Mech. Rock Eng.* **54**, 11–30 (2021).
19. Zhang, B. et al. Experimental and theoretical study on the dynamic effective stress of loaded gassy coal during gas release. *Int. J. Min. Sci. Technol.* **33**(3), 339–349 (2023).
20. Liu, H. et al. Mechanical evolution mechanism of coal and gas outburst. *Rock Mech. Rock Eng.* **52**, 1591–1597 (2019).
21. Soleimani, F. et al. Numerical modelling of coal and gas outburst initiation using energy balance principles. *Fuel* **334**, 126687 (2023).
22. Wold, M. B., Connell, L. D. & Choi, S. K. The role of spatial variability in coal seam parameters on gas outburst behaviour during coal mining. *Int. J. Coal Geol.* **75**(1), 1–14 (2008).
23. Shadrin, A. & Diyuk, Y. Geophysical criterion of pre-outburst coal outsqueezing from the face space into the working. *Int. J. Min. Sci. Technol.* **29**(3), 499–506 (2019).
24. Ma, Y. et al. Mechanism investigation on coal and gas outburst: an overview. *Int. J. Min. Metall. Mater.* **27**, 872–887 (2020).
25. Nie, B. et al. Insights into the nanoscale microstructure diversity of different rank coals. *Energy Fuels* **36**(18), 10899–10909 (2022).
26. Li, Z. et al. Multi-scale pore fractal characteristics of differently ranked coal and its impact on gas adsorption. *Int. J. Min. Sci. Technol.* **33**(4), 389–401 (2023).
27. Lu, S. et al. Numerical assessment of the energy instability of gas outburst of deformed and normal coal combinations during mining. *Process Saf. Environ. Protect.* **132**, 351–366 (2019).
28. Lu, Z., Wang, L., & Wu, S., et al. Investigation of pore structure and adsorption/desorption properties of coal in the non-uniform stress zone: implications for coal and gas outburst. *Natl. Resourc. Res.*, 2024: 1–22.
29. Nie, B. et al. Pore structure characterization of different rank coals using gas adsorption and scanning electron microscopy. *Fuel* **158**, 908–917 (2015).
30. Lu, G. et al. Influence of pore structure and surface free energy on the contents of adsorbed and free methane in tectonically deformed coal. *Fuel* **285**, 119087 (2021).
31. Qi, L. et al. Pore characterization of different types of coal from coal and gas outburst disaster sites using low temperature nitrogen adsorption approach. *Int. J. Min. Sci. Technol.* **27**(2), 371–377 (2017).
32. Guo, H. et al. Kinetic characteristics of desorption and diffusion in raw coal and tectonic coal and their influence on coal and gas outburst. *Fuel* **343**, 127883 (2023).
33. Wang, Z. et al. Characterization of pore structure and the gas diffusion properties of tectonic and intact coal: Implications for lost gas calculation. *Process Saf. Environ. Protect.* **135**, 12–21 (2020).
34. Zheng, J. et al. Degradation of mechanical and microporous properties of coal subjected to longterm sorption. *Fuel* **315**, 123245 (2022).
35. Cheng, M. et al. Effect of dynamic fragmentation on microscopic pore structure in coal: New insights into CH4 adsorption characteristics. *Fuel* **333**, 126228 (2023).
36. Jiang, J. et al. Study on the evolution of pore structure and desorption characteristics of crushed tectonic coals under the different conditions of unloading confining pressure. *Powder Technol.* **426**, 118681 (2023).
37. Jiang, B. et al. Effect of faults on the pore structure of coal and its resultant change on gas emission. *J. Pet. Sci. Eng.* **195**, 107919 (2020).
38. Barrett, E. P., Joyner, L. G. & Halenda, P. P. The determination of pore volume and area distributions in porous substances. I. Computations from nitrogen isotherms. *J. Am. Chem. Soc.* **73**(1), 373–380 (1951).
39. Landers, J., Gor, G. Y. & Neimark, A. V. Density functional theory methods for characterization of porous materials. *Colloids Surf. A Physicochem. Eng. Aspects* **437**, 3–32 (2013).
40. Lowell S, Shields J E, Thomas M A, et al. Characterization of porous solids and powders: surface area, pore size and density. Springer Science & Business Media, 2012.
41. Thommes, M. Physical adsorption characterization of nanoporous materials. *Chemie Ingenieur Technik* **82**(7), 1059–1073 (2010).
42. Jiang, C. L. Study of forming meichanism of outburst hole. *Chinese J. Rock Mech. Eng.* **19**(2), 225–228 (2000).
43. Thommes, M. et al. Physisorption of gases, with special reference to the evaluation of surface area and pore size distribution (IUPAC Technical Report). *Pure Appl. Chem.* **87**(9–10), 1051–1069 (2015).
44. Sun, W. et al. Fractal characterization and methane adsorption features of coal particles taken from shallow and deep coalmine layers. *Fuel* **155**, 7–13 (2015).

45. Zheng, Y. et al. Thermodynamic analysis of high-pressure methane adsorption on coal-based activated carbon. *Fuel* **230**, 172–184 (2018).
46. Yang, H. et al. Analytical and numerical research of stress intensity factor with a closed-crack in finite-rock-plates under biaxial compression. *J. Central South Univ. Sci. Technol.* **39**(4), 850–855 (2008).
47. Gdoutos E. E. *Fracture Mechanics: An Introduction*. Springer Nature, 2020.
48. Yang, H. et al. Effect shear stress criterion for closed-crack fracture. *Rock Soil Mech.* **29**(S1), 470–474 (2008).
49. Cao, P. et al. Mixed mode I/II fracture behavior of CSTBD sandstone specimen under different loading angles. *Geomech. Geophys. Geo-Energy Geo-Resour.* **9**(1), 54 (2023).
50. He, X. Q., Wang, E. Y. & Lin, H.-Y. Coal deformation and fracture mechanism under pore gas action. *J. China Univ. Min. Technol.* **25**(1), 6–11 (1996).
51. Xie, H. P. et al. Mining-induced mechanical behavior in coal seamsunder different mining layouts. *J. China Coal Soc.* **36**(7), 1067–1074 (2011).
52. Tu, Q. et al. Investigation of the formation mechanism of coal spallation through the cross-coupling relations of multiple physical processes. *Int. J. Rock Mech. Min. Sci.* **105**, 133–144 (2018).
53. Wang, L. et al. Detailed characterization of the pore and fracture structure and strength deg-radation mechanism of gas-containing coal. *Rock Soil Mech.* **42**(12), 3203–3216 (2021).
54. Xu, B., Xu, T., & Xue, Y., et al. Phase field modeling of mixed-mode crack in rocks incorporating heterogeneity and frictional damage. *Eng. Fracture Mech.*, 2024: 109936.
55. Li, W. & Chen, W. H. Initiation of near-surface I-II mixed mode cracks in fractured rocks subjected to hypohigh temperature and air-vapor pressure. *Chinese J. Rock Mech. Eng.* **42**(S1), 3206–3218 (2023).
56. Zhao, Y. et al. Cracking and stress–strain behavior of rock-like material containing two flaws under uniaxial compression. *Rock Mech. Rock Eng.* **49**, 2665–2687 (2016).
57. Muskhelishvili, N. I. *Some basic problems of the mathematical theory of elasticity* (Noordhoff, 1953).
58. Hou, B. et al. Hydraulic fracture initiation theory for a horizontal well in a coal seam. *Pet. Sci.* **10**, 219–225 (2013).
59. Li, D. et al. Mechanical behaviors and acoustic emission fractal characteristics of coal specimens with a preexisting flaw of various inclinations under uniaxial compression. *Int. J. Rock Mech. Min. Sci.* **116**, 38–51 (2019).
60. Gao, M. et al. Mechanical behavior of coal under different mining rates: A case study from laboratory experiments to field testing. *Int. J. Min. Sci. Technol.* **31**(5), 825–841 (2021).
61. Kumari, W. G. P. et al. Temperature-dependent mechanical behaviour of Australian Strathbogie granite with different cooling treatments. *Eng. Geol.* **229**, 31–44 (2017).

Acknowledgements

This research was financially supported by the National Natural Science Foundation of China (52104073).

Author contributions

P.Z. led the writing of the manuscript. A.Y.Y. provided the funding. B.Z. conducted the experiment and collected the data. H.Q.L. provided theoretical analysis. K.J. and H.Z. performed the data processing.

Declarations

Competing interests

The authors declare no competing interests.

Additional information

Correspondence and requests for materials should be addressed to A.Y.

Reprints and permissions information is available at www.nature.com/reprints.

Publisher's note Springer Nature remains neutral with regard to jurisdictional claims in published maps and institutional affiliations.